sciendo

Mathematical Modelling in Civil Engineering
Vol. 15-No. 2: 20-32-2019
Doi: 10.2478/mmce-2019-0006

ON THE USE OF THE CUBIC TRANSLATION TO MODEL BIMODAL WIND PRESSURES

François Rigo - PhD Student, Wind Tunnel Lab, University of Liège, Belgium and F. R. S.-FNRS, National Fund for Scientific Research, Belgium, e-mail: francois.rigo@uliege.be
Thomas Andrianne – Lecturer, PhD, Wind Tunnel Lab, University of Liège, Belgium, e-mail: t.andrianne@uliege.be
Vincent Denoël – Lecturer, PhD, Structural & Stochastic Dynamics, University of Liège, Belgium, e-mail: v.denoel@uliege.be

Abstract: The cubic translation model is a well know tool in wind engineering, which provides a mathematical description of a non-Gaussian pressure as a cubic transformation of a Gaussian process. This simple model is widely used in practice since it offers a direct evaluation of the peak factors as a function of the statistics of the wind pressure data. This transformation is rather versatile but limited to processes which are said to be in the monotonic region. For processes falling outside this domain, this paper describes an alternative which is based on the physics of the wind flow. First, it is shown, with a classical example of a flow involving corner vortices on a flat roof, that the pressure data which does not meet the monotonic criterion is in fact associated with a bimodal distribution. Then, the proposed approach is to decompose this data into the two governing modes (slow background turbulence and fast corner vortices) and apply the usual translation model to each of them.

Keywords: peak factor – non Gaussianity – wind tunnel tests – low-rise building – monotone criterion

1. Introduction

This work focuses on the statistical analysis of wind pressures, involving significant non-Gaussianity, in the scope of building roofs. Peak factor estimation is necessary for the prediction of wind loads and thus the design of structures. The precision of wind tunnel measurements is necessary to keep important information: high sampling frequency, fine tap spatial distribution, long samples. With the increasing of pressure sensors precision in terms of sampling frequency, local effects can be better captured; however the question can be raised about the relevance of very local effects, negligible in term of spatial and time scale compared to the entire structure.

Many research works have been carried about the non-Gaussian statistics analysis of wind pressure [1, 2, 3, 4, 5]. Their purpose is to estimate peak factors, based on the translation process [6]. Peak factor can be estimated using the Hermite moment-based model [7] applied to the Gaussian peak factor of the classical peak factor model [8]. This Hermite moment-based approach relies on a transformation of a Gaussian into a non-Gaussian softening process (cubic translation) [4]. For many wind pressures, there is a good correlation between the peak factor g and high-order statistics (skewness γ_3 and kurtosis γ_4).

There exist also more advanced models, such as the modified Hermite model [9] or the revised Hermite model [10] which are able to deal with stronger non-Gaussianity. The former is quite heavier to solve due to a non-linear system; the latter requires conditions on γ_3 and γ_4. However, the Hermite moment-based model is less precise when pressures are significantly non-Gaussian. The cubic translation model requires the process to satisfy the monotone condition [11]. Peng [12] proposes a mapping of statistics in the (γ_3, γ_4) plane to reach the monotone condition by adjusting their value but the physical interpretation is less easy.

Another kind of solution is a point-to-point distribution function mapping between Gaussian and non-Gaussian processes, assuming a Weibull or Gamma distribution [2]. This model allows to obtain an analytical evaluation of the peak factor but only in the case of a Weibull or Gamma distribution and is not general enough to handle multiple mode distributions. Indeed, wind pressure

on a low-rise building roof can be highly non-Gaussian and present different modes: e.g. the turbulent background and a component linked to the main flow behavior (corner vortices). By studying the probability density function (PDF), such modes can be highlighted, together with the analysis of higher rank properties such as the autocorrelation. An accurate separation of the modes makes it possible to select the process of interest in the tail of the distribution and to restore the good agreement between g and (γ_3, γ_4) by satisfying the monotone condition. This is the option that is followed in our study.

The main contribution of the paper is to propose a solution for the treatment of significantly non-Gaussian pressure processes, thanks to a new way to separate the different contributions in the wind flow and to estimate peak factors based on long time wind pressure measurements. High-order and rank statistics are studied, and instead of adjusting skewness and kurtosis through mapping, we suggest dealing with these processes by first de-mixing the wind pressure process, and then applying a cubic translation model to the tail component. By doing so, the peak factor predicted by the model (after de-mixing) is not only computable with the model but also in much better agreement with the peak factor obtained with statistical treatment of long data series. The general methodology that is proposed to decompose the wind pressure. The developed methodology will be illustrated with the analysis of wind pressure measurement on a square low-rise building flat roof, with a 45° wind orientation but can be applied to other practical cases of wind around buildings that require an estimate of wind loads on areas. After understanding the kind of flow involved and basic pressure statistics, the de-mixing methodology is explained. Then, processes with bimodal distributions are simulated to deduce statistical parameters violating the monotone condition. A parallel between autocorrelation and probability distribution decomposition is applied to decompose the pressure into simple components. Finally, it is shown that usual peak factor formulations are sufficiently accurate to model extreme values.

2. Case study

The setup made by Blaise et al. [13] consists of a square plan-form low-rise building (sides of 45 m and a height of 25 m), uniformly instrumented by 121 pressure taps in a quarter of its roof (see Figures 1 and 2), sampled at $f_s = 500$ Hz. The model is placed at an incidence of 45° in the atmospheric boundary layer test section of the wind tunnel (WT) of the University of Liege. This direction is fixed to obtain a symmetry in the complex nature of the corner vortices developed at the edges [14].

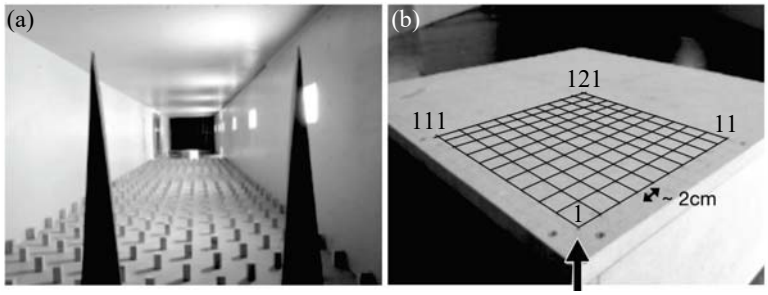

Fig. 1 - (a) Model inside the WT, (b) location of pressure taps on the model (wind direction fixed at 45°).

The atmospheric boundary layer test section creates a turbulent wind of category III according to the Eurocode [15], with $z_0 = 0.3$ m and $z_{min} = 5$ m. The mean velocity (Equation (1)) and turbulence intensity (Equation (2)) profiles are presented in Figure 2.

$$U_\infty(z) = U_{ref} k_r \ln(z/z_0), k_r = 0.19(20z_0)^{0.07}, \quad (1)$$

$$I_u(z) = \frac{1}{\ln\left(\frac{z}{z_0}\right)}. \quad (2)$$

Pressure taps are linked to the scanner using pneumatic connection (vinyl tubes) of internal diameter of 1.32 mm and length 600 mm. The static pressure is well measured but unsteady components have

to be dynamically corrected, thanks to the theoretical formulation of Bergh and Tijdeman [16] and the experimental apparatus of Rigo [17]. Figure 3 presents the transfer function, in amplitude and phase, necessary to correct measurements, until the sampling frequency of 500 Hz.

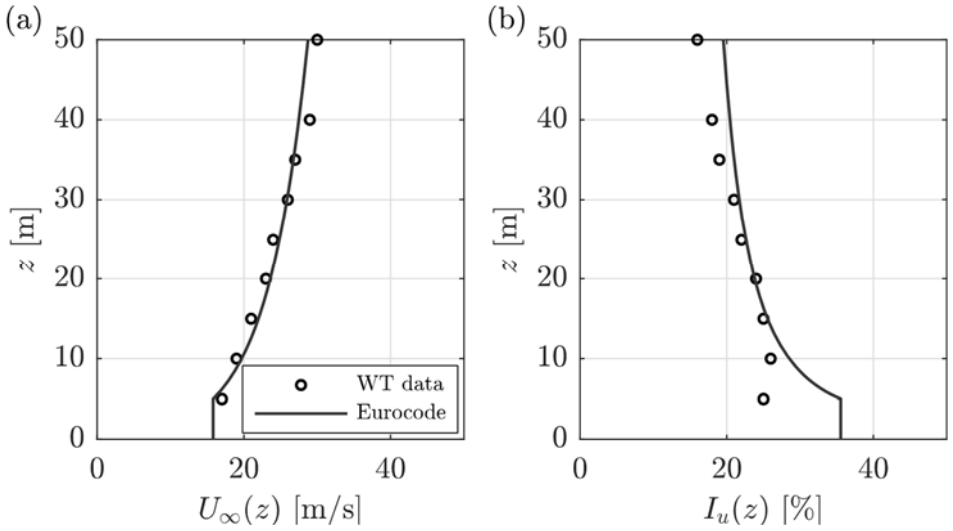

Fig. 2 - (a) Mean velocity $U_\infty(z)$ and (b) turbulence intensity $I_u(z)$ profiles of the atmospheric boundary layer: measurements and comparison with suburban category III terrain, from Eurocode (1991), (Blaise et al. (2017)).

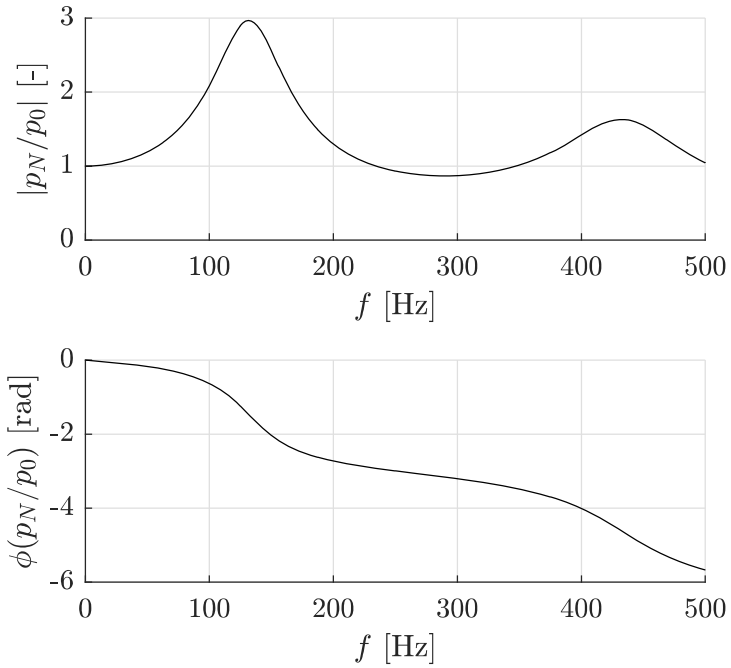

Fig. 3 - Transfer function of the pressure tubes, in amplitude and phase of corrected pressure as a function of the frequency [16, 17]

2.1. WT results: First rank statistics

The geometric scaling is $\lambda_L = 1/100$. The Reynolds condition would require a velocity scaling of $\lambda_U = \lambda_L^{-1} = 100$, which would impose WT speed of about 1000 m/s, impossible. The Reynolds dependency is more critical for smooth and mainly circular shapes such as cylinder or sphere. When the flow is completely separated and turbulent, the Strouhal scaling is preferred. Because of WT performances, the velocity scaling is chosen as $\lambda_U = 1/3.5$. The Strouhal condition imposes $\lambda_T = \frac{\lambda_L}{\lambda_U} = 1/28.6$ (time).

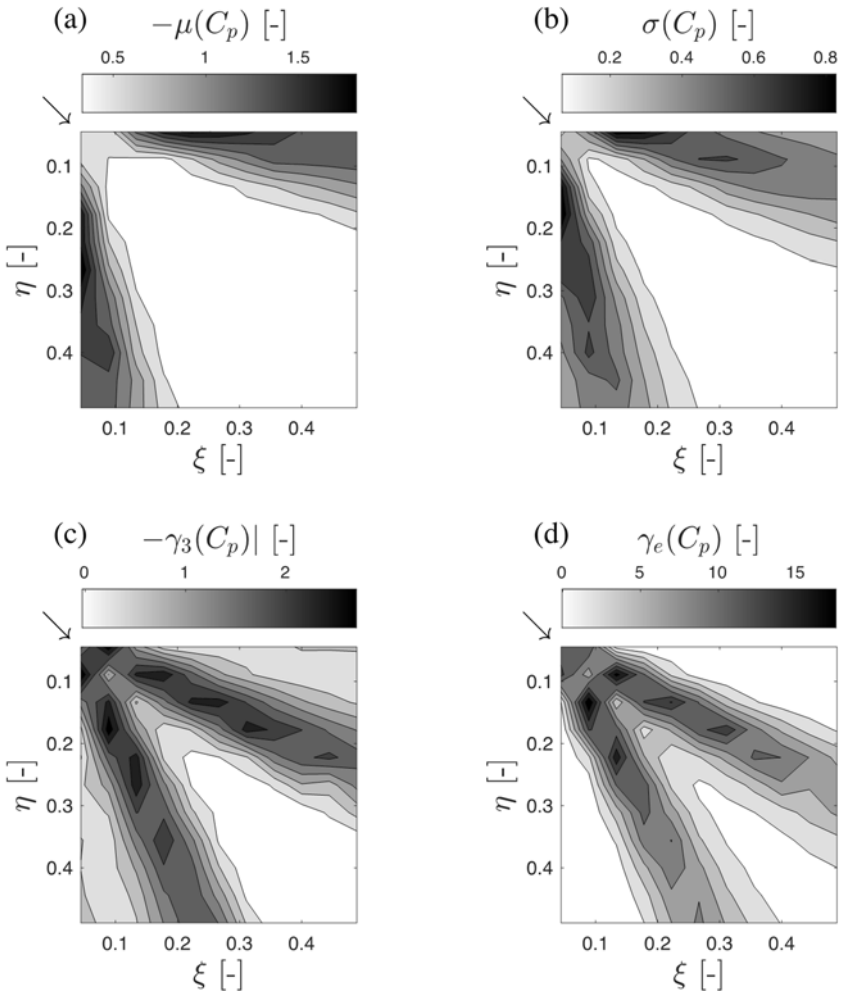

Fig. 4 - Map of (a) mean, (b) standard deviation, (c) skewness and (d) kurtosis (excess).

Every measurement is converted in full scale. A total of 13 h of measurement has been taken in the WT, corresponding to 371.8 h full scale. This long information allows to compute precise PDF tail, necessary to study the extreme values. In the following, statistics are presented in a non-dimensional way: position $(\xi, \eta) = (x/L, y/L)$ and pressure coefficient with Equation (3).

$$C_p = \frac{p - p_\infty}{\frac{1}{2}\rho U_\infty^2} \tag{3}$$

The Reynolds number of the WT model is 6.8×10^5. The flow around this low-rise building is characterized by corner vortices, that roll in a cone shape. The pressure is mainly negative because of the separated nature of the flow ($\mu(C_p)$ in Figure 4(a)) and is the most negative where it starts to separate, just after the edges, on the corner. The two cones on both corners have a main axis, recognizable by the ridgelines of the standard deviation of the pressure coefficient $\sigma(C_p)$, in Figure 4(b). The non-Gaussianity happens in the corner vortices boundaries, where $|\gamma_3(C_p)|$ and $|\gamma_e(C_p)|$ are the highest. For a Gaussian process, $\gamma_3 = 0$ and $\gamma_4 = 3$. The excess $\gamma_e = \gamma_4 - 3 = 0$. On Figure 4, a lower right triangle appears systematically, with low statistics values. This region is mainly Gaussian, with a low dispersion and mean pressure value. Physically, the flow in this region is the case of a simple turbulent flow on a flat plate. This region is not studied here, since it has smaller extreme values and represents less interest compared to the complex flow in corner vortices. As suggested by Kawai and Nishimura [14], there is one main vortex at the corner, but a secondary small one develops just next to the edge, below the main vortex. Pressure taps in this setup were not close enough to the edge to capture well this secondary vortex. Nevertheless, in Figure 4, $\gamma_3(C_p)$ increases just next to the edge, at $(\xi, \eta) = (0.05, 0.4)$, suggesting the presence of another vortex. By looking at skewness and kurtosis values, each pressure distribution in the corner

vortices has a negative skewness (negative extreme pressure events) and a positive excess kurtosis (called softening process, the PDF has a flatter shape compared to a Gaussian process). Figure 5 shows a typical pressure coefficient signal (at tap 4): with local negative extreme pressures ($\gamma_3 < 0$) and wide range of distributed values, no concentrated values around the mean. Moreover, the two modes are identifiable with two principal levels at around $C_p = -0.9$ and -2.1.

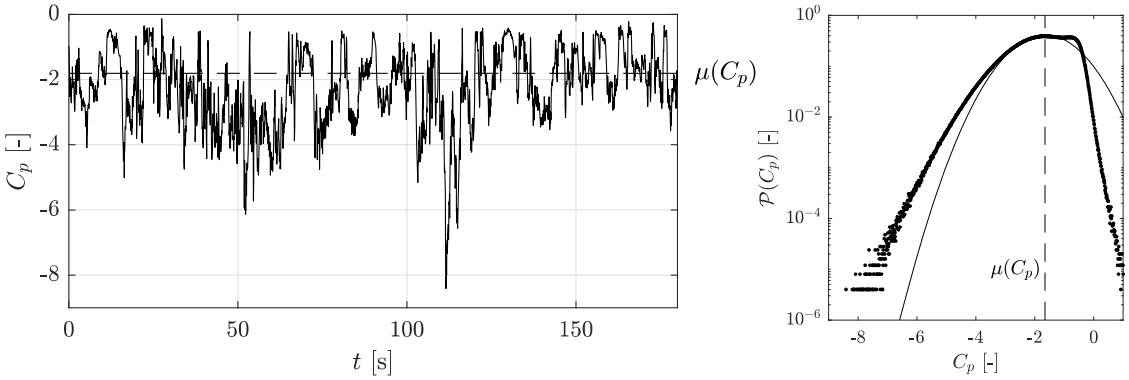

Fig. 5 - Pressure signal at tap 4 and PDF (log-scale).

Figure 6 allows to have a quick qualitative view of the PDF. Each PDF is represented in log-scale at all 121 pressure tap locations. The same scaling is used to represent them and have a quick comparative view of the dispersion and asymmetry of PDFs. Those in the corner vortices are highly non-Gaussian and two modes (two bumps) are clearly identifiable. This motivates the discussion of Section 4.

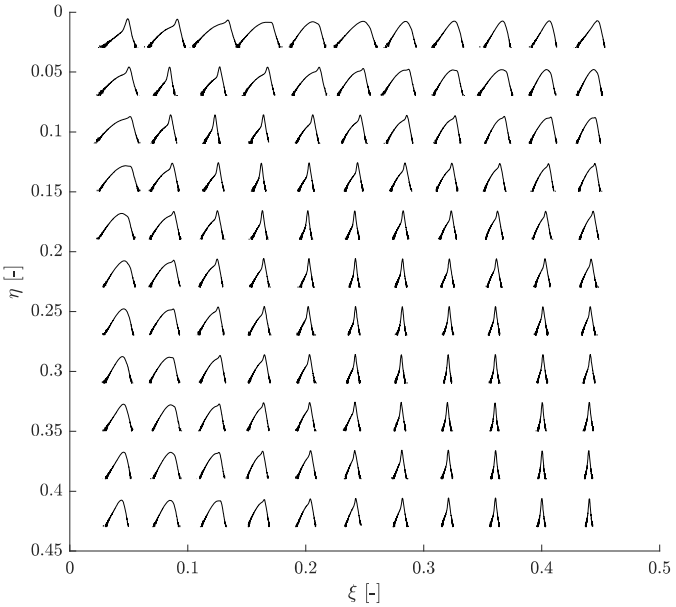

Fig. 6 - Map of all PDFs.

2.2. Extreme values

As done for pressure coefficient signal, it is possible to compute statistics and draw probability density functions for extreme (peak) pressures. Based on time series, the peak value of $\boldsymbol{C_p}$ over a time window $\boldsymbol{T}$ (conventionally 10 min full-scale) is taken. This operation is repeated for the whole signal so that the peak pressure is not unique and has a distribution. Figure 7 shows PDF of extreme pressures for taps 56 to 60, which cross the corner vortices region: (i) close to the edge (56), the pressure is significantly negative, (ii) in the corner vortices region (from tap 57 to 59), the extreme distribution is wider, (iii) after the corner vortices, where only background turbulence remains, the peak pressure is less negative and its distribution narrow.

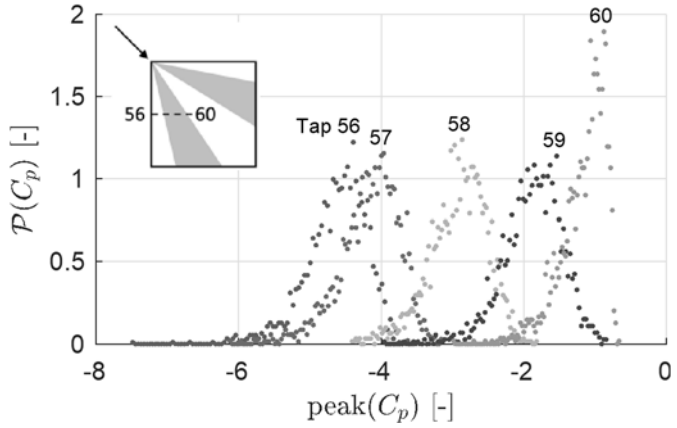

Fig. 7 – PDF of peak pressure coefficient (10 min windowing) in corner vortices region.

The peak factor is computed as $g = \max_T \left|\frac{C_p - \mu}{\sigma}\right|$. Figure 8(a) shows a map of the mean value of peak factor of the pressure coefficient $\mu_g(C_p)$, the highest values happening were the vortex cone touches the roof, similarly to γ_3 and γ_e.

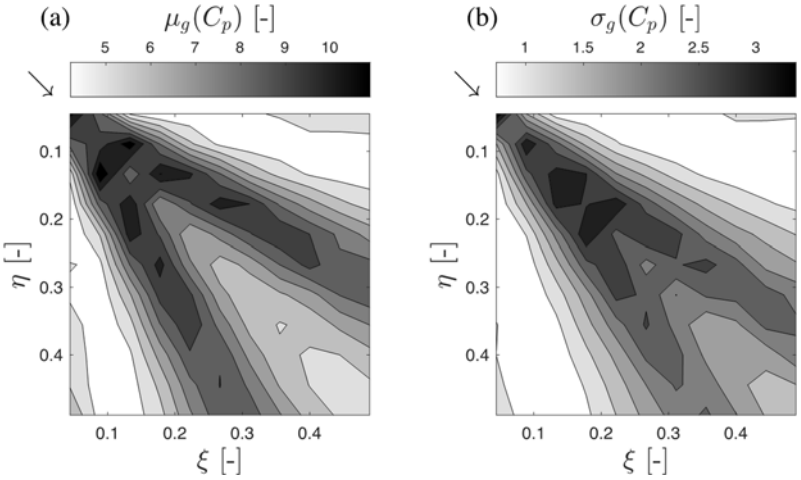

Fig. 8 - Map of peak factor (a) mean and (b) standard deviation.

2.2. Cubic translation and peak factor estimation

A usual way to estimate peak factors from pressure measurement uses cubic translation from a Gaussian process u to a non-Gaussian (softening) one x [7]: the Hermite moment-based model,

$$x = \kappa\left[u + \sum_{n=3}^{\infty} h_n H_{n-1}(u)\right] \approx \kappa[u + h_3(u^2 - 1) + h_4(u^3 - 3u)] \tag{4}$$

where κ is a scale factor that ensures x has unit variance and H_n is the n^{th} Hermite polynomial. A softening process is characterized by a wider tail in the distribution compared to a Gaussian one (*i.e.* with $\gamma_e > 0$). Most of wind pressure measured on buildings and roofs are softening processes. The mean peak factor is computed by [1],

$$\begin{aligned} g_{nG} = \mu_{g_{Her}} = \kappa\Bigg\{\left(\beta + \frac{\gamma}{\beta}\right) + h_3\left[\beta^2 + 2\gamma - 1 + \frac{1.98}{\beta^2}\right] \\ + h_4\left[\beta^3 + 3\beta(\gamma - 1) + \frac{3}{\beta}\left(\frac{\pi^2}{6} - \gamma + \gamma^2\right) + \frac{5.44}{\beta^3}\right]\Bigg\} \end{aligned} \tag{5}$$

where h_3, h_4, κ are coefficients of moment-based Hermite model [7], the Euler's constant is $\gamma \approx 0.5772$, and

$$\beta = \sqrt{2\ln(\nu_0 T)}, \quad \nu_0 = \sqrt{\frac{m_2}{m_0}}, \quad m_i = \int_0^\infty n^i S_y(n) dn, \quad h_3 = \frac{\gamma_3}{4+2\sqrt{1+1.5\gamma_4}}, \quad h_4 = \frac{\sqrt{1+1.5\gamma_4}-1}{18}, \quad \kappa = \frac{1}{\sqrt{1+2h_3^2+6h_4^2}} \tag{6}$$

where ν_0 is the mean zero upcrossing rate of process y (standardized non-Gaussian process obtained from a non-Gaussian process x, $y = (x - E[x])/\sigma_x$), T is the duration, m_i is the i^{th} spectral moment of y, $S_y(n)$ is the one-sided power spectral density of y, n is the frequency in Hz. The validity range of the application of Hermite model is defined in a monotonic region, *i.e.* corresponding to a monotone transformation of $x(u)$, requiring $\frac{dx}{du} > 0$, satisfying [4, 11],

$$\gamma_e \geq (1.25\gamma_3)^2 \tag{7}$$

This boundary is shown in Figure 9(a), where pressure taps in the lower region are not eligible. These taps a represented on the roof in Figure 9(b), precisely in the corner vortices region.

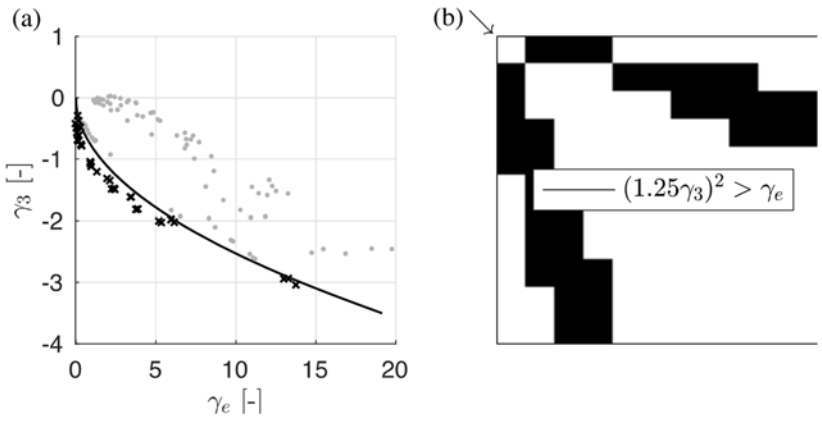

Fig. 9 - (a) Skewness and kurtosis pairs of all taps (• taps inside the limit and × outside), with the monotone limit (solid line), (b) Taps outside the limit.

Choi [18] studied the different regions and monotone limits of Hermite-based model (for softening and hardening processes). Strong negative wind pressures measured on buildings and roofs are mostly softening processes. In our case, taps falling outside the monotone limit are in region III of Figure 10(a). Choi [18] proposes to overcome this limit by taking a softening-hardening-softening transformation (Figure 10(b)) in order to keep an increasing (monotone) transformation $x(u)$ and cross the decreasing part of the softening process. This technique requires a hybrid model depending on the value of x and deform the nature of the process.

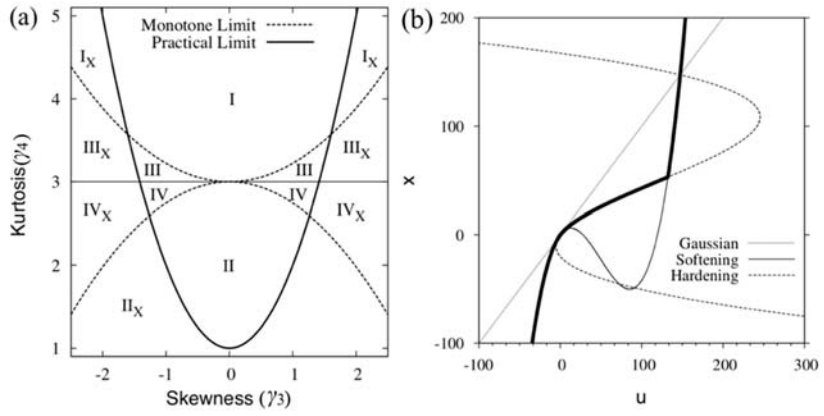

Fig. 10 - (a) Regions of Hermite model applicability, (b) Region III of Fig. 10a: softening-hardening-softening truncation for monotone transformation $x(u)$ (Choi (2010)).

Another methodology to deal with these processes is proposed in the next section, based on physical interpretation in the case of bimodal processes.

For processes inside the monotone region, Yang [19] computes bias and sampling errors of peak factor estimation based on translation process models. Davenport [8] suggests that Gaussian processes are assumed to have a small variability of the extreme distribution. On contrary, non-Gaussian processes exhibit a large variability in extreme (for either positive or negative skewness). Yang [19] suggested to compute the variance of the non-Gaussian peak factor g_{nG}, to take into account the sampling errors of estimated skewness and kurtosis (because of a limited length of data) that leads to errors in the translation model function and thus peak factor estimation.

$$\mathrm{Var}(g_{nG}) = \sigma_{g_{Her}}^2 = \left(\frac{\partial g}{\partial \gamma_3}\right)^2 \mathrm{Var}(\gamma_3) + \left(\frac{\partial g}{\partial \gamma_4}\right)^2 \mathrm{Var}(\gamma_4) + 2\frac{\partial g}{\partial \gamma_3}\frac{\partial g}{\partial \gamma_4}\mathrm{Cov}(\gamma_3, \gamma_4) \tag{8}$$

Kareem and Zhao (2011) estimated the variance of the peak factor for a softening process (related to Equation (5)),

$$\sigma_{g_{Her}}^2 \cong \kappa^2 \left\{ \frac{\pi^2}{6\beta^2} + 6.58h_3^2 + 9h_4^2\left[1.64\beta^2 + \frac{12.69}{\beta^2} + 5.32\right] + 6.58\frac{h_3}{\beta} + 6h_4\left[\frac{2.66}{\beta^2} + 1.64\right] + 12\, h_3 h_4\left[1.64\beta + \frac{2.66}{\beta}\right]\right\} \tag{9}$$

3. Methodology: de-mixing and adaptation to the cubic model

Pressure processes in the corner vortices region are highly non-Gaussian and bimodal. Based on this physical interpretation, instead of using the whole PDF in a non-monotone transformation, we propose to use only the mode of interest in the cubic model: the one containing the tail. Each PDF has thus first to be decomposed.

Cook [20] proposed to model the wind pressure data as a sum of several components, the Skew Gaussian Exponential Mixture Model (SGEMM). Inspired by this model, we suggest modeling the wind pressure as a mixture of two skew-Gaussian (SG) distributions. The skew-gaussian (SG) is given by

$$p_{SG}(x) = 2\phi\left(\frac{x-\xi}{\omega}\right)\Phi\left(\alpha\frac{x-\xi}{\omega}\right) \tag{10}$$

where ϕ and Φ are the standard gaussian PDF and cumulative density distribution (CDF), ξ a location parameter, ω a scale parameter and α a skewness parameter. It is also possible to use another distribution, the skew-hyperbolic secant, to fit only the tail but we keep only two SG distributions thanks to the physical interpretation: (i) mode 1 corresponding to the turbulent background flow (as the one present on the roof region without vortex) and (ii) mode 2 to the corner vortices fluctuation (separated flow). The resulting PDF is the weighted combination of those distributions,

$$P(x) = w_1 p_1(x) + w_2 p_2(x) \tag{11}$$

where w_i are weighted parameters. Standard adjustment methods would recommend proceeding to a non-linear least-squares fitting to find appropriate estimates of 8 model parameters, under the constraint $w_1 + w_2 = 1$. In the case of a bi-modal PDF, the mean and the variance of the total PDF can be linked to those of its components 1 and 2,

$$\mu = w_1\mu_1 + w_2\mu_2, \text{ with } w_1 + w_2 = 1 \tag{12}$$

$$\sigma^2 = w_1\sigma_1^2 + w_2\sigma_2^2 + w_1w_2(\mu_1 - \mu_2)^2 \tag{13}$$

When bumps are clearly identifiable, initial guesses for the location and scale parameters (ξ, ω) are easy to choose and the fitting converges quickly.

Standard adjustment methods work well when the modes are easy to identify but can be ill-conditioned in some limit cases (e.g. same average and/or standard deviation for two modes). In this case, a more robust method is necessary. The idea comes from a physical interpretation of the modes from a timescale point of view. Close to edges of buildings, two phenomena are involved in the pressure, a mixture between a slow background turbulence (mode 1) and a fast shedding (mode 2), which is visible in the autocorrelation function of the mixed process as a kink in the shape. The autocorrelation is defined by:

$$R(t_1, t_2) = \iint_{-\infty}^{+\infty} (x_1 - \mu)(x_2 - \mu)P_x(x_1, x_2, t_1, t_2)\mathrm{d}x_1\mathrm{d}x_2 \tag{14}$$

where $P_x(x_1, x_2, t_1, t_2)$ is the probability to have the pressure coefficient $x = x_1$ at t_1 and $x = x_2$ at t_2. In a mixture model, the random variable is either in mode 1 or mode 2. The pressure coefficient can be represented by,

$$c_p(t) = w_1(t)c_{p,1}(t) + w_2(t)c_{p,2}(t) \tag{15}$$

where $w_i(t)$ = 1 if c_p is in mode 1, and 0 otherwise. The weight has thus also a certain dynamics, and probability distribution $P_{w_1}(i, j, t_1, t_2)$ where i at time t_1 and j at time t_2 are equal to 0 or 1. We have $P_{w_1}(1,0, t_1, t_2) = P_{w_2}(0,1, t_1, t_2)$. The signal being stationary, we can rewrite the autocorrelation depending on $\tau = t_1 - t_2$,

$$\begin{aligned} R(\tau) = {} & P_{w_1}(1,1,\tau)R_1(\tau) + P_{w_1}(0,0,\tau)R_2(\tau) + P_{w_1}(1,1,\tau)(\mu_1^2 - 2\mu\mu_1) \\ & + P_{w_1}(0,0,\tau)(\mu_2^2 - 2\mu\mu_2) + 2P_{w_1}(1,0,\tau)(\mu_1\mu_2 \\ & - \mu(\mu_1+\mu_2)) + \mu^2 \end{aligned} \tag{16}$$

The general expression of the autocorrelation is thus based on the sum of two decreasing exponentials, the autocorrelation of each mode,

$$R_i(\tau) = \sigma_i^2 e^{-\tau/\tau_i} \tag{17}$$

where τ_i is the characteristic time of mode i $(i = 1, 2)$. Two limit cases are interesting to analyze:

$$\lim_{\tau\to 0} R(\tau) = \bar{w}_1R_1(0) + \bar{w}_2R_2(0) + \bar{w}_1\bar{w}_2(\mu_1 - \mu_2)^2 \tag{18}$$

where $\bar{w}_i$ is the mean of $w_i(t)$. Equation 15 is consistent with Equation 12.

$$\lim_{\tau\to\infty} R(\tau) = \bar{w}_1^2R_1(\tau \to \infty) + \bar{w}_2^2R_2(\tau \to \infty) = 0 \tag{19}$$

It is thus possible to fit the autocorrelation as a sum of two decreasing exponentials. When the mean pressures in both modes are close to each other (standard methods are ill-conditioned), the third term in Equation (15) is negligible and by identifying the two components in the autocorrelation function, it is possible to extract at $\tau = 0$ the weighted variance of each mode and use them as an additional constraint in the fitting. Figure 11 summarizes the autocorrelation-aided de-mixing methodology in two modes. Once the bi-modal distribution is properly de-mixed, the peak factor estimation is performed using the model of Kareem and Zhao [1] on Mode 2 only (the one associated to the most negative pressures).

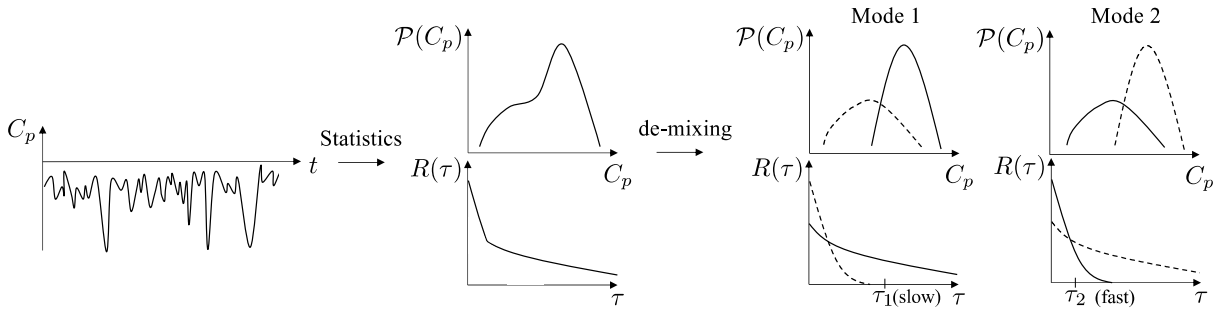

Fig. 11 - Autocorrelation-aided de-mixing methodology.

4. Results

Figure 12 shows the decomposition in modes of the PDF at pressure tap 4. The two modes are easy to identify by looking at the two bumps in the PDF (Figure 12(a)). Figure 12(b) show that the de-mixing algorithm and modes identification is not susceptible to the duration of measurement, only the tail is limited to probability of 10^{-4}. While the computation of peak factor directly from data requires long measurements, the peak factor estimation from de-mixing is quicker. Figure 13(a) show the PDF at tap 11, modes are almost superimposed and less easy to identify. The autocorrelation (Figure 13(b)) is decomposed in two modes and the weighted variance of each mode is extracted from the value at the origin to constrain the PDF fitting.

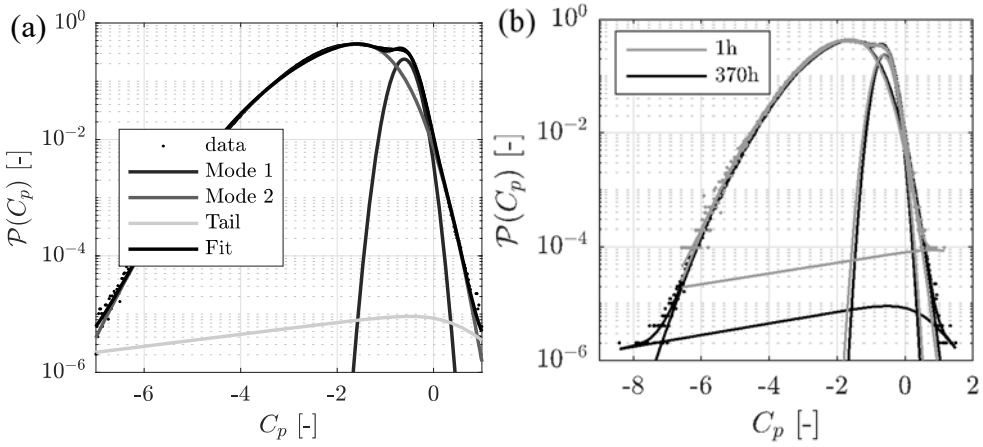

Fig. 12 – Tap 4: (a) PDF decomposition in mode 1, 2, tail (log-scale) and (b) influence of duration measurement.

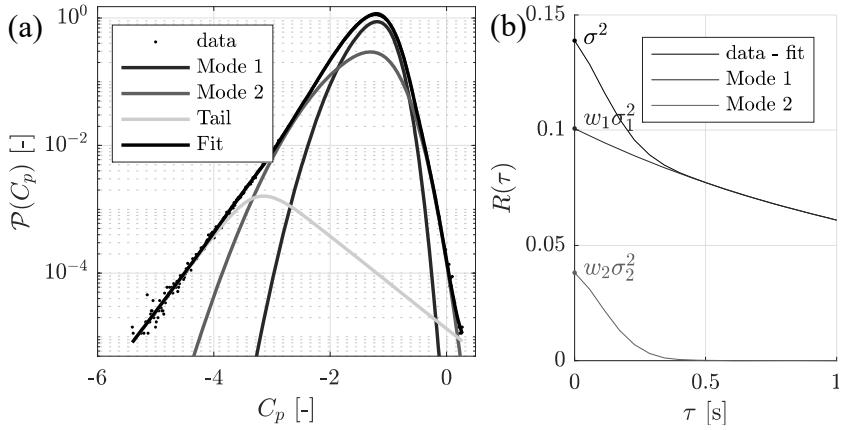

Fig. 13 – Tap 11: (a) PDF decomposition in mode 1, 2, tail (log-scale) and (c) autocorrelation decomposition in modes 1 and 2.

In the case of bimodal distribution, even the sum of two nearly Gaussian can be highly non-Gaussian and does not meet the criterion. It is possible to study that by simulating non-Gaussian bimodal distribution using Ornstein-Uhlenbeck processes. This is done in Figure 14, where the skewness-kurtosis ((a) and (c)) map is represented with the monotone limit. The two modes are generated separately with a given mean and standard deviation. The weight (transition) between both modes $w_1(t)$ is also generated randomly with 0 or 1 values, such that the resultant is computed using Equation (14).

In parallel with $\gamma_3 - \gamma_e$ map results, the associated density distributions with simulated signals is represented in (b) and (d). Characteristics of mode 1 are kept (mean and standard deviation, physically associated to the turbulence) and the mean of mode 2 is changed in (b) (more negative, with a constant standard deviation). The higher the mean difference between both modes, the more likely the skewness increases, and the criterion is no more met. This can also be observed in (d), where the mean is kept and the standard deviation of mode 2 is increased. This is clearly in accordance with the characteristics of pressure processes present is the corner vortices and justify the de-mixing of them.

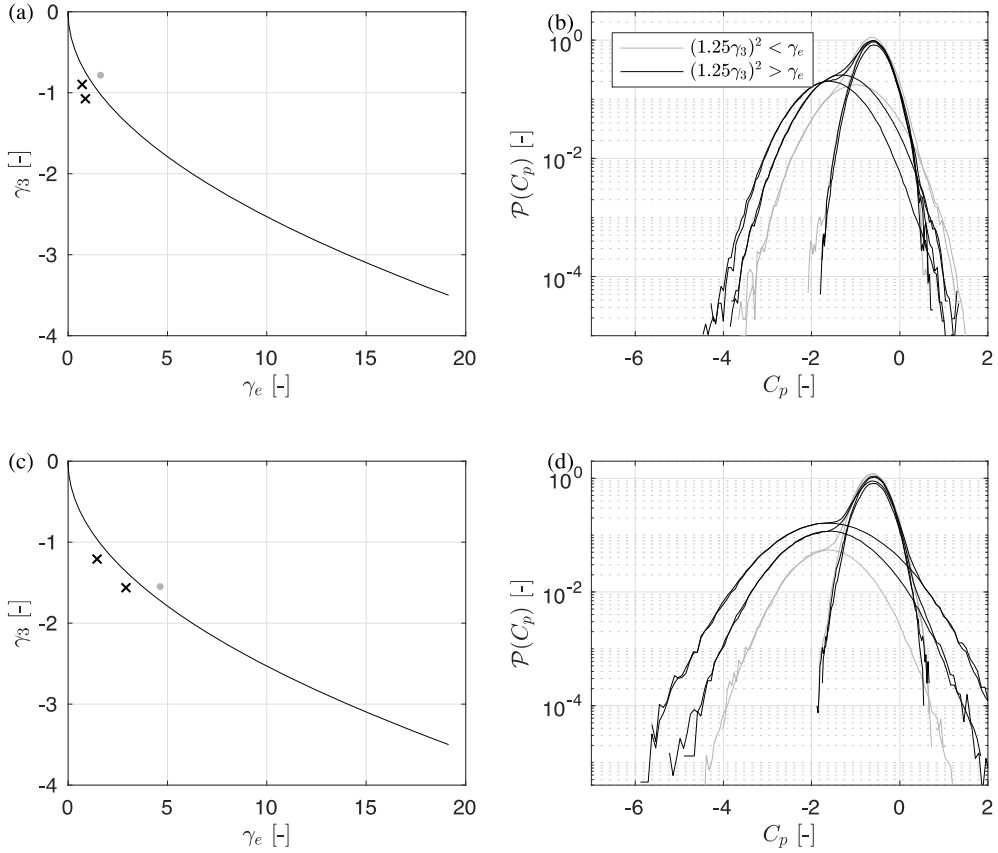

Fig. 14 – Simulation of bimodal processes: Regions of Hermite model applicability in skewness-kurtosis map by changing (a) the mean of mode 2 and (c) its variance. Corresponding density distributions (b) and (d), drawn for both modes p_1, p_2 and the resultant (weighted sum) P.

Figure 15 compares results (a) before and (b) after de-mixing: the taps outside the monotone limit (before de-mixing) are used in the de-mixing methodology and the skewness-kurtosis map of each mode is reproduced. The monotone criterion is fulfilled for all taps after de-mixing: (i) Mode 1 represents the background turbulence and is almost Gaussian (low γ_3 and γ_e) while (ii) Mode 2 associated to corner vortices and peak pressure is more non-Gaussian but still inside the monotone region. Figure 15(c) shows the peak factor estimation compared to the measured one without and with de-mixing. Thanks to the decomposition, the statistics used from mode 2 allows to satisfy the monotone limit and improve the peak factor estimation.

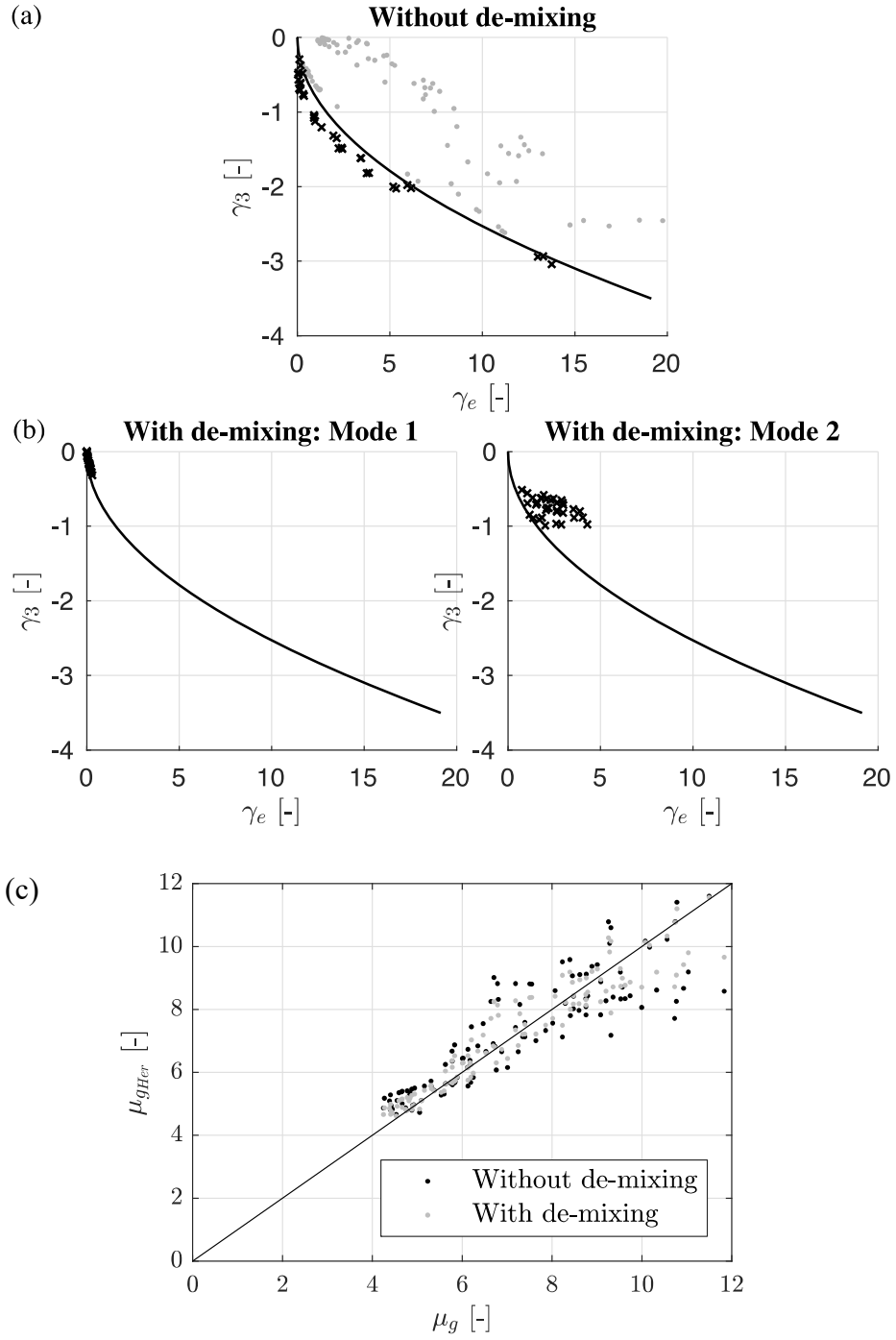

Fig. 15 – De-mixing methodology results: (a) skewness-kurtosis monotone region (a) before de-mixing (● taps inside the limit and × outside) and (b) after de-mixing of taps that were outside in (a) for the two modes, (c) peak factor estimation improvement.

5. Conclusions

In conclusion, in order to correct peak factor estimations based on cubic translation model, strong non-Gaussian pressure processes that are not inside the monotonic region have been corrected by decomposing their PDF into two competing sources of wind pressure, associated to different known physical phenomena: (1) the fast shedding in separated regions (corner vortices) and (2) the slow background turbulence. Mode 2 is responsible for large negative peaks and is therefore the relevant one to estimate peak factors using Hermite moment-based model. Doing so provides a much better agreement with long time series.

Acknowledgements The authors want to thank the Belgian National Fund for Scientific Research (FNRS) for their support.

This article was presented at the 2nd National Conference on Wind Engineering, June 6-7, 2019, Bucharest, Romania.

References

[1] Kareem, A., and Zhao, J. (1994). Analysis of non-Gaussian surge response of tension leg platforms under wind loads, J. offshore Mech. and Arctic Eng., ASME, 116, 137-144.

[2] Sadek, F., and Simiu, E.(2002). Peak non-Gaussian wind effects for database-assisted low-rise building design, J. Eng. Mech., ASCE, 128(5), 530-539.

[3] Chen, X. and Huang, G. (2009). Evaluation of peak resultant response for wind-excited tall buildings. Engineering Structures 31, 858-868.

[4] Kwon, D.K. and Kareem, A. (2009). Peak Factors for Non-Gaussian Load Effects Revisited, J. Struct. Eng., 137(12): 1611-1619.

[5] Huang, M., Huang, S., Feng, H., Lou, W. (2016). Non-Gaussian time-dependent statistics of wind pressure processes on a roof structure. Wind and Structures an International Journal. 23. 275-300.

[6] Grigoriu, M. (1984). Crossings of non-Gaussian translation processes, *J. Eng. Mech.*, ASCE, 110(4), 610-620.

[7] Winterstein, S.R.(1987) Moment-based Hermite models of random vibration, Lyngby, Report No. 219. Department of Structural Engineering, Technical University of Denmark, Lyngby, Denmark.

[8] Davenport, A. G. (1964). Note on the distribution of the largest value of a random function with application to gust loading, J. Inst. Civ. Eng., 24, 187-196.

[9] Tognarelli, M. A., Zhao, J. and Kareem, A. (1997). Equivalent statistical cubicization for system and forcing nonlinearities, J. Eng. Mech., ASCE, 123(8), 1772-1790.

[10] Winterstein, S. R., Ude, T. C. and Kleiven, G. (1994). Springing and slow-drift responses: predicted extremes and fatigue vs. simulation, Proc. BOSS-94, 3, MIT, 1-15.

[11] Winterstein, S.R. and MacKenzie, C.A. (2012). Extremes of nonlinear vibration: models based on moments, L-moments, and maximum entropy, J.Offshore.Mech. Arct., 135(2), 021602.

[12] Peng, X., Luping Yang, L., Gavanski, E., Gurley, K. and Prevatt, D. (2014). A comparison of methods to estimate peak wind loads on buildings, J. Wind Eng. Ind. Aerodyn., 126, 11–23.

[13] Blaise, N., Andrianne, T., and Denoël, V. (2017). Assessment of extreme value overestimations with equivalent static wind loads, J. of Wind Engineering and Industrial Aerodynamics 168, 123– 133.

[14] Kawai, H., Nishimura, G. (1996). Characteristics of fluctuating suction and conical vortices on a flat roof in oblique flow, J. Wind Eng. Indus. Aerodyn. 60, 211–225.

[15] Eurocode, E. EN 1991-1-3: Actions on Structures-General Actions-Wind Actions. European Committee for Standardization.

[16] Berg, H., Tijdeman, H. (1965). Theoretical and experimental results for the dynamic response of pressure measuring systems. National Aero and Aeronautical Research Institute, NLR-TR F.238.

[17] Rigo, F. (2017). Unsteady pressure measurement around aerodynamic bodies: Development of a calibration apparatus and wind tunnel testing. Master's dissertation, University of Liège.

[18] Choi, M. and Sweetman, B. (2010). The Hermite Moment Model for Highly Skewed Response with Application to Tension Leg Platforms, ASCE Journal of Offshore Mechanics and Arctic Engineering, 132, Issue 2.

[19] Yang, Q., Chen, X., Liu, M. (2019). Bias and sampling errors in estimation of extremes of non-Gaussian wind pressures by moment-based translation process models, Journal of Wind Engineering and Industrial Aerodynamics, Volume 186, Pages 214-233.

[20] Cook., N.J. (2016). On the gaussian-exponential mixture model for pressure coefficients, Journal of Wind Engineering and Industrial Aerodynamics, 53, 71–77.

[21] Rigo, F., Andrianne, T. and Denoël, V. (2018). Mixture model in high-order statistics for peak factor estimation on low-rise building. In Proceedings of the 15th Conference of the Italian Association for Wind Engineering, Naples, Italy.